scientific reports

Check for updates

OPEN

A simple phenomenological account for the metal-induced crystallization of amorphous Ge and Si films

A. R. Zanatta

When combined with certain metal species, films of amorphous Ge or Si can have their typical crystallization temperatures decreased, by a factor of three or four, down to ~ 200 °C. The phenomenon is called metal-induced crystallization (MIC) and, since its first observation in the late 1960's, shows a great technological potential in producing (poly-)crystalline films of Ge or Si onto low-melting point substrates under reduced energy conditions. From the scientific point of view, the microscopic mechanisms behind the MIC phenomenon (still) represents a scientific challenge, where most of the proposed models are invariably influenced by the samples details giving the impression that they only apply to very specific metal–semiconductor combinations and/or circumstances. The lack of a simple–unified explanation of the MIC mechanism in amorphous Ge and Si films, allied to its technological importance, gave rise to this work. Accordingly, the paper starts by presenting some crucial aspects of the MIC phenomenon, as obtained from the investigation of amorphous Ge and Si films codeposited with some metals. In order to be inclusive, the experimental results of various metal–semiconductor bi-layered samples are also presented and discussed in detail. Based on the main aspects of these two (codeposited and bi-layered) metal–semiconductor systems, a simple phenomenological model is proposed to explain the MIC of amorphous Ge and Si films. The model relies on some basic chemical aspects (like electron distribution, orbital features, and bonding character) of the different atom species to account for the metal–semiconductor interaction and consequent amorphous-to-crystalline transformation. According to it, the metals presenting "extra–free" electrons into their outermost orbitals are the most effective in promoting an atom-bonding rearrangement and, therefore, in reducing the crystallization temperature of the amorphous Ge and Si films.

One of the first studies relating the effect of metal species on the atomic structure of semiconducting compounds was performed in the late 1950's and it was named recrystallization because of the improvement (the already crystalline) CdS films experienced after being covered with a thin Ag layer and heated to 500–600 °C[1]. The study evolved to other II–VI semiconductors and various metal layers, and the role of the metals in promoting the crystal improvement of the films was suggested to be that of providing an alternative path for the process—either by the formation of an intermediate compound or by the development of defects[2,3].

Similar investigations were carried out on amorphous Ge and Si films as well[4–6]. This time, however, the focus was the temperature of the amorphous-to-crystalline transformation of the films. In view of the extraordinary results these investigations provided, according to which the typical crystallization temperature T_{cryst} of metal-free Ge (~ 600 °C) and Si (~ 800 °C) films could be reduced to approx. 200 °C when combined with certain metals, the phenomenon was called metal-induced crystallization (MIC)[7]. Since the beginning it became clear that, in addition to the metal–semiconductor interaction, the MIC mechanism usually requires an external source of energy to take place. Most of this energy supply is thermally-based, so it can range from simple thermal annealing treatments to others involving the use of electric fields[8], or either laser[9] or microwave radiation[10], for example. Furthermore, considering the enormous potential of MIC in achieving (poly-)crystalline Ge or Si films under reduced thermal budgets, the MIC mechanism was explored targeting applications such as thin film transistors and flat panel displays[11,12], data storage media[13,14], and photovoltaic cells[15,16], just to mention a few of them.

Within this context, the combination of the metals Al[17–20] and Ni[21–24] with amorphous Si films (in the form of metal-onto-semiconductor bi-layered structures) have been, by far, the most studied systems. The literature also

Institute of Physics, University of São Paulo, São Carlos 13560-590, SP, Brazil. email: zanatta@ifsc.usp.br

presents results of the metal−Ge system[4–6], and (much less) studies regarding the MIC of codeposited samples (i.e., corresponding to systems in which the metal and the semiconductor are deposited simultaneously)[25–28]. As a consequence of this "unbalanced" research work, but mostly because of the complexity involving the MIC of the Ge and Si films—that comprises details about the sample (film codeposited or in the layered form), the metal (type and amount), the annealing conditions (origin, temperature and time), the characterization method, etc.—different interpretations have been proposed to account for the MIC phenomenon. Even though most of these explanations sound appropriate, they are invariably influenced by the samples particulars and filled with plenty of jargons—interface-controlled phenomena, (inter-)diffusion, critical thickness, catalyst, nucleation site, grain boundary, compound (eutectic, germanide, silicide) formation, etc.—suggesting that the proposed mechanisms can only be applied to very specific metal−semiconductor combinations and/or circumstances.

Just to illustrate the point, hitherto, the most comprehensive experimental studies of the MIC of amorphous Ge and Si films were carried out by Knaepen et al.[29,30]. These studies comprise a detailed investigation (by means of in-situ x-ray diffraction, in the 100–900 °C temperature range) of the atomic structure of amorphous Ge and Si films covered with 23 different metals (in the form of metal−semiconductor bi-layers). According to these studies (that are perfectly in accordance with many others[7]), the mechanisms behind the MIC of the amorphous Ge and Si films can be divided into two main groups (namely, eutectic-related and compound-forming) that are driven by the canonical *"reduction of the free energy associated with the transformation of amorphous Ge or Si into their (poly-)crystalline counterparts"*. However, as will be shown in the following sections, in spite of the very same sample preparation and characterization procedures[29,30], a closer look at these two proposed MIC mechanisms give the impression that they are inadequate and/or that they proceed very differently in the amorphous Ge and Si films. In particular, as stated in the compound-forming mechanism: whereas the MIC takes place in amorphous Si only after the advent of the Si-rich most stable phase of the corresponding silicide, the MIC of amorphous Ge does not always involve the Ge-rich germanide phases (without mentioning the exceptions relating the Cr, V, Nb, Mo, Ta, Re and W metals)[30]. Apparently, it happens because of differences in the solubility and/or in the diffusivity of the elements (either metal or Ge or Si atoms) as the annealing temperature advances. However, it is well-known that the MIC phenomenon takes place in systems presenting a clear metal−semiconductor interface (bi-layers) and—with absolute no difference—in codeposited amorphous films, where the concepts of solubility and/or of diffusion do not, necessarily, should be a concern. Regarding the so-called eutectic-related MIC mechanism, it originates from the common knowledge that certain metals do not form germanides with Ge and silicides with Si. Nevertheless, since the MIC occurs before the eutectic point (i.e., $T_{cryst} < T_{eut}$): what is the connection? Besides, why two different MIC mechanisms (one taking place before the eutectic point, and the other after the germanide/silicide formation)? Indeed, at the present stage, it seems that: whatever the proposed mechanism (compound-forming or eutectic-related or involving another peculiar−exclusive characteristic), it is always possible to find a (very convenient) metal−semiconductor association without explaining the real origin of the MIC phenomenon.

The above scenario, in which a simple−unified description of the MIC mechanism in amorphous Ge and Si films is still missing, forms the basis of this work. With this in mind, the paper presents and discusses the essentials of the MIC phenomenon that, in combination with the experimental results provided by amorphous Ge and Si films codeposited with some metals and in the form of metal−semiconductor bi-layered samples, allow to propose a simple phenomenological model to unravel the MIC phenomenon. According to it, an atom-bonding rearrangement mechanism, as induced by the most external electrons in the metal species, plays a decisive role in reducing the crystallization temperature of the metal−semiconductor systems.

Experimental results and discussion

Figure 1 presents a few selected experimental data obtained from Ge (upper panels) and Si (lower panels) films prepared by the radio frequency sputtering technique (see the "Materials and Methods" section for details). The results correspond to films codeposited with different metals (Fig. 1a, b, e and f) and in the metal-free form (Fig. 1c, d, g and h). The typical crystallization temperatures T_{cryst}'s of the metal-free Ge (~ 500 ± 50 °C) and Si (~ 750 ± 50 °C) films are also indicated for comparison purposes. The results show the influence of the metal species (type and amount) and annealing time onto the T_{cryst} of the amorphous Ge and Si films, along with some representative Raman spectra.

At first sight, Fig. 1 contains several notable aspects: (1) *metal type* or *nature* (Fig. 1a, e)—indicating the effect of different metals onto the MIC of the Ge and Si films—with no apparent relationship between T_{cryst} and the corresponding metal atomic number; (2) *metal concentration* (Fig. 1b, f)—that, besides the type, the metal concentration also exerts great influence onto the MIC phenomenon (in fact, as it will be shown in the following, this is behind the almost nil MIC effect verified in the $GePb_{0.8\%}$ film (Fig. 1a)); (3) *treatments conditions* (Fig. 1c, g)—even though relating the metal-free amorphous Ge and Si films, the time extent of the thermal annealing treatments greatly affects the crystallization process—which prompts serious doubts about the effectiveness of the MIC mechanism when involving long (in the range of hours) thermal treatments; and (4) *crystallization criterion* (Fig. 1d, h)—indicating that, in certain cases (either because of the samples details or treatments conditions, or a combination of them), the crystallization of the Ge or Si films can be only partial. Most of these aspects are crucial to achieve the MIC of the Ge and Si films (in both codeposited and bi-layered metal−semiconductor samples), so they will be considered separately.

The *metal type* or *nature* represents the main core of this work in the sense that it is supposed to decide the metal−semiconductor interaction and, ultimately, the mechanisms behind the MIC phenomenon (Fig. 1a, e). The subject will be discussed in further detail in sequence.

Concerning the *metal concentration*, whereas it can be precisely controlled just in the codeposited films (Fig. 1b, f), in the metal−semiconductor bi-layered samples the metal content is determined, ideally (i.e., apart from the metal solubility limit and/or atom diffusion issues), by the thickness of the metal layer. The

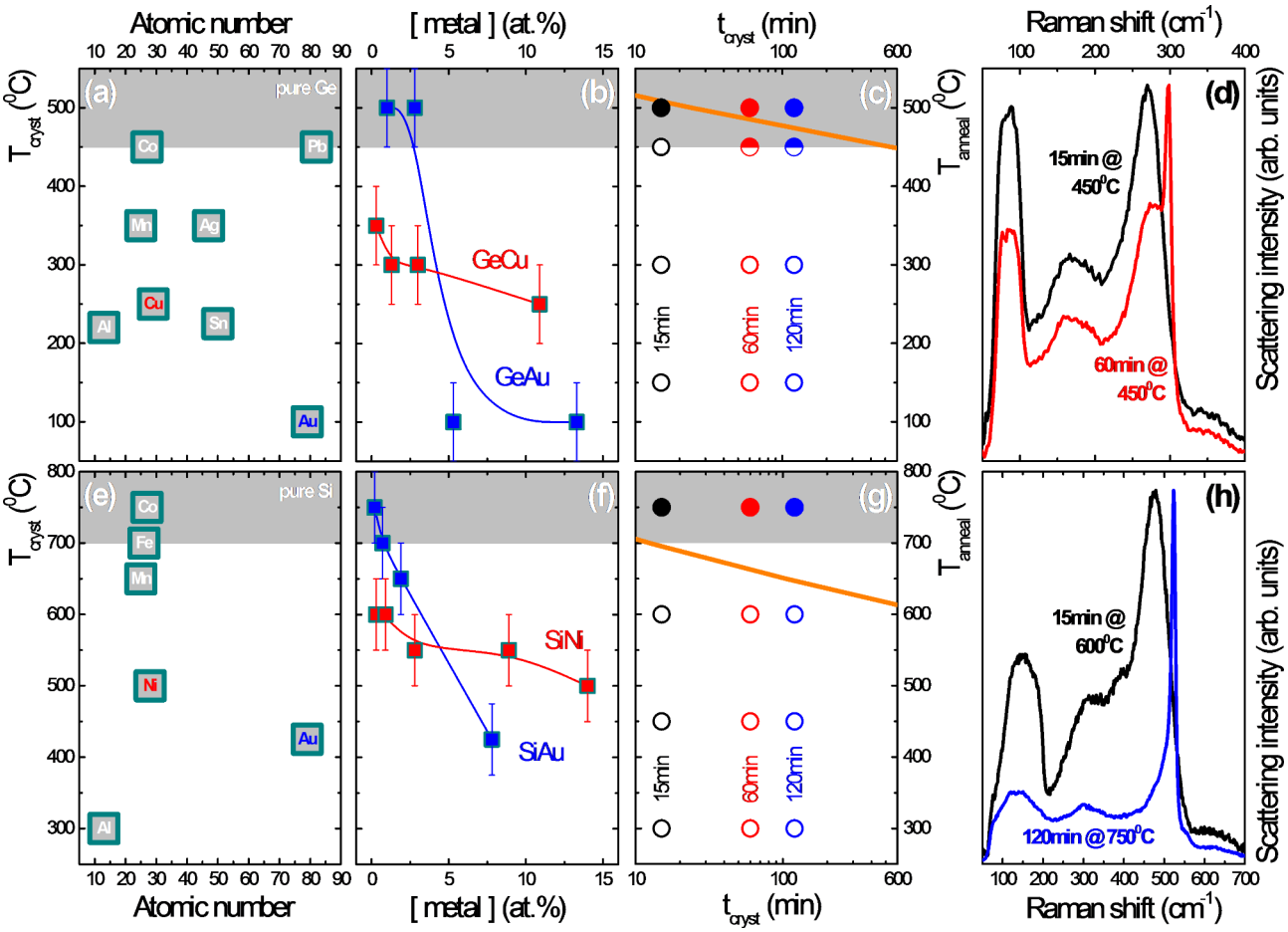

Fig. 1. Collection of experimental data achieved from Ge (upper panels) and Si (lower panels) films prepared by radio frequency sputtering. The typical range of the crystallization temperatures T_{cryst}'s of the metal-free Ge (~ 500 ± 50 °C) and Si (~ 750 ± 50 °C) films are indicated in shadow gray. The data correspond to: the T_{cryst} *versus* the atomic number of some metals as obtained from the Ge (a) and Si (e) films; the T_{cryst} *versus* the concentration of Cu and Au in the Ge films (b) and of Ni and Au in the Si films (f); and the annealing temperature T_{anneal} *versus* annealing time t_{cryst} of the Ge (c) and Si (g) metal-free films. The lines joining the experimental data in (b) and in (f) are just guides to the eye. For clarity reasons, error bars (typical experimental T_{cryst} ± 50 °C) were indicated only in (b) and in (f). The symbols in (c) and in (g) indicate that the films are: amorphous (open symbols), partially crystallized (semi-filled), and crystalline (filled). The solid straight lines in (c) and in (g) correspond to the results of Blum and Feldman[31,32]. The Raman spectra of the Ge (d) and Si (h) metal-free films after thermal annealing at some selected temperatures-times are also shown.

presence of metal species alters the physico-chemical environment of the disordered Ge or Si atomic network. Assisted by an external energy supply (mostly of thermal origin), this metal–semiconductor interaction will induce the local reordering of the Ge or Si atoms, which performance is expected to be proportional to the number of metal atoms available. Not rarely, this local crystallization (around the metal species) can propagate to the rest of the amorphous network—either because of metal migration (as a result of the metal expulsion from the local amorphous-to-crystal transformation) or simply due to structural crystal replication. Both the *metal concentration* and the *treatments conditions* of the samples have a decisive influence in the initiation and propagation of the MIC phenomenon: the former determining the extent of the (originally) amorphous Ge or Si regions, and the latter providing the best energy conditions (temperature and time) to advance the necessary structural changes (crystallization and/or metal atom diffusion). Essentially, the MIC of the amorphous Ge and Si films is a thermodynamically-based process in which the crystallization is enhanced as a result of the metals presence. Although presenting the data of metal-free amorphous Ge and Si, the role played by the *treatments conditions* onto the crystallization of the films is shown in Fig. 1c, g. As can be seen, without any metal, the films remain amorphous after treatments below ~ 400 °C (Ge films) and ~ 700 °C (Si films)—independent of the annealing time. Under these temperature + time conditions (or integrated thermal budget) the energy supply is not enough to produce any crystallization of the films. Also, whereas thermal annealing the Ge films at ~ 450 °C for 15 min produces no crystallization, treatments for 60 and 120 min induce their partial crystallization. The results of Blum and Feldman[31,32] are also shown for comparison (solid straight lines in Fig. 1c, g), illustrating that the crystallization temperature can be reduced by ~ 50 °C (Ge films) and ~ 100 °C (Si films) simply by

increasing the annealing time from 10 min to 10 h. In this respect, experiments involving annealing treatments for long times[33–35] not only makes the MIC phenomenon technologically unattractive but (without clearly showing the results of the metal-free samples) may contribute with misleading information. Another important feature that is evident from Fig. 1c, g—but that can be observed quite often in the literature—refers to small differences in the T_{cryst} values. In most of the cases they arise because of differences in the samples main characteristics (codeposited, layered, metal concentration, etc.), annealing procedures, and/or derive from the adopted *crystallization criterion*. While the crystallization process itself is supported by well-established standard methods (such as microscope-based investigations, spectroscopic techniques, etc.) the definition of T_{cryst} can be somehow ambiguous. In particular, when considering the microscope-based investigations: does the observed crystallization represent a sizeable amount of the film? does T_{cryst} indicate the total or partial crystallization of the film? is it possible to clearly separate the MIC results from those originated from the usually mandatory specimen handling procedure (cutting, milling, thinning)? A similar reasoning applies to other methods (x-ray diffraction, Raman scattering, optical spectroscopy, etc.) and, therefore, the *crystallization criterion* (or *criteria*) should be as detailed as possible. The importance of the *crystallization criterion* is illustrated in Fig. 1d, h that shows the Raman spectra of metal-free Ge and Si films after different thermal annealing conditions. According to them, whereas the atomic structure of the films Ge (15 min @ 450 °C) and Si (15 min @ 600 °C) are amorphous—as clearly indicated by the presence of broad features in the Raman spectra—increasing the time and/or temperature of the annealing treatment can produce either the partial Ge (60 min @ 450 °C) or total Si (120 min @ 750 °C) crystallization of the films. Consequently, since differences are expected in the MIC studies, a typical $T_{cryst} \pm 100$ °C (comprising some data dispersion, the experimental error, and small variations in defining T_{cryst}) sounds appropriate when evaluating the MIC results provided by different metal–semiconductor samples and/or authors.

Being aware of the above aspects, henceforth, this work will consider the MIC results of Ge and Si films codeposited with different metal species, and thermally annealed in the ~ 150–750 °C temperature range. For practical reasons, only the films containing the highest amount of metal will be presented. The atomic structure of the films (both metal-free and alloyed with different metals) was investigated by Raman spectroscopy involving low laser power conditions, a typical optical penetration depth of ~ 500 nm, and the measurement of several different regions. Furthermore, T_{cryst} was associated to the temperature at which the crystallization starts by assuming a ± 50 °C uncertainty (see the "Materials and Methods" section for further details).

In addition to the results given by the codeposited Ge and Si films, this work also considers the data of Knaepen et al.[29,30] corresponding to 30 nm thick metal films (Al, Ti, V, Cr, Mn, Fe, Co, Ni, Cu, Zr, Nb, Mo, Ru, Rh, Pd, Ag, Hf, Ta, W, Re, Ir, Pt or Au) on top of 200 nm thick amorphous Ge and Si films i.e., of metal–semiconductor bi-layered samples. The atomic structure (in the 100–900 °C temperature range) of the samples was studied by means of x-ray diffraction, and the T_{cryst}'s correspond to the maximum intensity variation of either the Ge(220) or Si(111) diffraction peaks. In this case, the crystallization of the metal-free Ge- and Si layers took place, respectively, at 600 and 800 °C. Again, the details of these samples and experiment can be found in the "Materials and Methods" section. An overview of the results regarding the bi-layered samples is presented in Fig. 2: metal–Ge samples (upper panels) and metal–Si samples (lower panels). These are just exploratory representations that will be useful in the following.

For discussion purposes, the T_{cryst}'s of the metal–semiconductor bi-layered samples are displayed as a function of: the metal melting temperature T_{melt} (Fig. 2a, e)[36], the temperature of eutectic formation T_{eut} (Fig. 2b, f)[37], the temperature of germanide T_{germ} (Fig. 2c)[38] or silicide T_{silic} formation (Fig. 2g)[39,40], and the metal Debye temperature T_{Debye} (Fig. 2d, h)[41]. Additionally, the T_{cryst} values were grouped according to the electron configuration (or rows in the Periodic Table of the Elements) of the species considered[42], i.e.: **[Ne] core** (corresponding to Al and Si), **[Ar] core** (Ti, V, Cr, Mn, Fe, Co, Ni, Cu, and Ge), **[Kr] core** (Zr, Nb, Mo, Ru, Rh, Pd, Ag), and **[Xe] core** (Hf, Ta, W, Re, Ir, Pt, and Au). Other graphical representations (involving the atomic number, the standard atomic weight, the atomic radius, the density, the electron binding energy, the electron first ionization energy, the work function, and the Pauling's electronegativity of all metal species) were also made and they can be seen in SuppInfo_Part1. The T_{cryst} results of the codeposited samples (not shown for clarity reasons) are similar to those of Fig. 2 and they will be considered soon.

Without explicitly revealing the origin of the MIC phenomenon, the data of Fig. 2 contain several relevant information: (1) T_{cryst} *versus* T_{melt} (Fig. 2a, e)—given that $T_{cryst} < T_{melt}$, the MIC of amorphous Ge or Si films is essentially a solid-state process (i.e., it does not involve the formation of any obvious liquid phase). (2) T_{cryst} *versus* T_{eut} (Fig. 2b, f)—the crystallization of the amorphous Ge or Si films always take place at temperatures lower than that required to form the corresponding binary eutectic compound (i.e., $T_{cryst} < T_{eut}$). In fact, it seems that the MIC–T_{eut} association has much more historical[4] than logical reasons (that is, "*formation of a low-temperature eutectic melt caused by the lowering of the binary eutectic temperature when one of the two components is amorphous*"—that has never been convincingly proved[43]). (3) T_{cryst} *versus* T_{germ} (Fig. 2c) and T_{cryst} *versus* T_{silic} (Fig. 2g)—it is obvious that the MIC of the films occurs nearby the temperature of the germanide or silicide formation. Even so, in view of the data scatter (around the $T_{cryst} = T_{germ}$ and $T_{cryst} = T_{silic}$ reference lines), and variety of germanide/silicide phases (as indicated by the extent of the horizontal error bars), it is not possible to draw any further (reliable) conclusion. Moreover, as stated before, this germanide/silicide formation "theory" in assisting the MIC of Ge/Si films presents some problems: (3a) it is frequently associated with an improved atom diffusion across the metal–semiconductor interface (and/or nearby crystal-seeds and/or grain-boundaries[7,29,30]—depending on the convenience), but the MIC phenomenon also takes place in codeposited samples where, in principle, all (metal and Ge or Si) atoms are close together; and (3b) considering that, occasionally, the MIC phenomenon can be observed before the detection of any germanide/silicide phase, it is not perfectly clear if the germanide/silicide appearance influences the MIC process, or if it just happens (see SuppInfo_Part2, that shows the development of Cu_3Ge and $NiSi_2$ only after the crystallization of Cu–Ge and Ni–Si codeposited films). At this point we

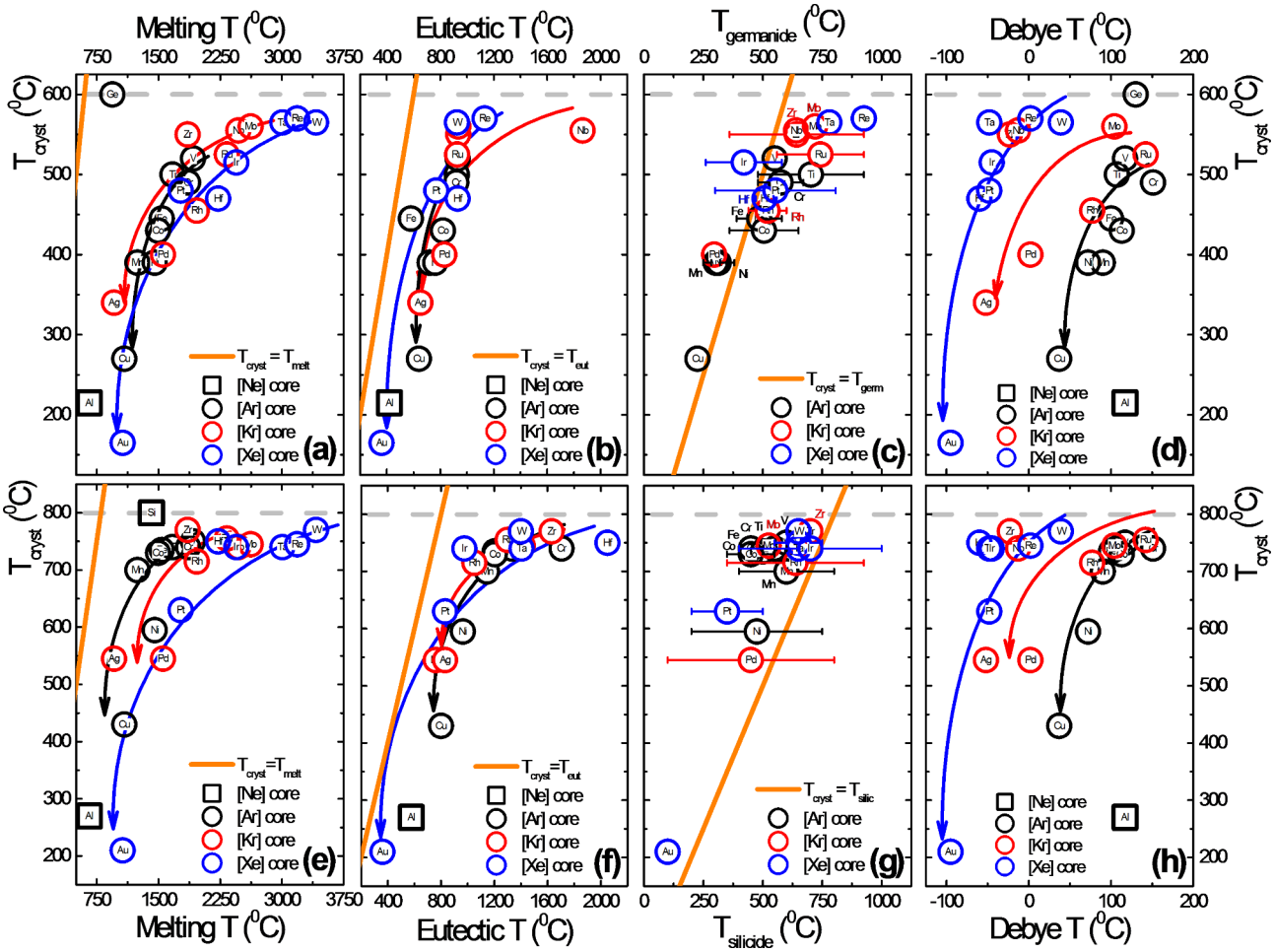

Fig. 2. Crystallization temperature T_{cryst} of metal–Ge (upper panels) and metal–Si (lower panels) bi-layered samples, as obtained by Knaepen et al.[29,30]. The T_{cryst}'s of the metal-free Ge (~ 600 °C) and Si (~ 800 °C) samples are denoted by the dashed horizontal gray lines. The T_{cryst} values are represented as a function of: the metal melting temperature T_{melt} (a) and (e); the temperature of eutectic formation T_{eut} (b) and (f); the temperature of germanide T_{germ} (c) or silicide T_{silic} (g) formation; and the metal Debye temperature T_{Debye} (d) and (h). The thick straight (orange) solid lines correspond to: $T_{cryst} = T_{melt}$ (a) and (e); $T_{cryst} = T_{eut}$ (b) and (f); and $T_{cryst} = T_{germ}$ (c) and $T_{cryst} = T_{silic}$ (g). The thin (black, red, and blue) solid-arrowed lines are just guides to the eye (d) and (h). The error bars in (c) and (g) indicate the minimum/maximum temperature of germanide or silicide formation (no matter what phase).

cannot ignore that this apparent absence of T_{cryst} *versus* T_{melt}, T_{eut}, T_{germ}, and T_{silic} relationship may be due to the fact that: whereas the present T_{cryst}'s refer to metal–semiconductor bi-layered samples[29,30], most of the other temperatures come from either crystalline or amorphous bulk materials—the only exception being the T_{germ} data obtained from metal films onto amorphous Ge films[38]. (4) T_{cryst} *versus* T_{Debye}—the same reasoning applies to the T_{Debye} (that correlates the materials elastic properties with their thermodynamic characteristics such as thermal expansion and conductivity, specific heat, and lattice enthalpy[44]) that, once more, does not present a straightforward connection with the T_{cryst} values (Fig. 2d, h). This time, however, it is possible to distinguish a systematic reduction of T_{cryst} as the number of valence electrons increases within each of the considered periods or groups (i.e., **[Ne] core**, **[Ar] core**, etc.). Strictly, this behavior seems to be quite common but, in certain cases, it is more remarkable as in Fig. 2d, h and in Fig. 1a, b, d, e, f, h of SuppInfo_Part1.

An alternative way to perceive this behavior more clearly is by representing T_{cryst} in terms of the number of electrons occupying the outermost orbitals n_{out} (i.e., beyond the noble gas core or configuration). This is shown in Fig. 3, that displays the results from the metal–semiconductor bi-layered samples[29,30] (just as before arranged according to their electron configuration), as well as those obtained from codeposited Ge and Si films (this work—codepos) and from other authors (Ge films—Oki et al.[4], and Si films—Herd et al.[6]). In addition to the clear T_{cryst} reduction observed at increasing n_{out} values, the figure also presents some data scatter. It arises because of differences in the characteristics of the samples and experimental procedure but, typically, this dispersion stays in the $T_{cryst} \pm 50$–100 °C range—particularly, when considering the T_{cryst} of the metal-free codeposited films (not shown): ~ 500 °C for Ge and ~ 750 °C for Si (Fig. 1).

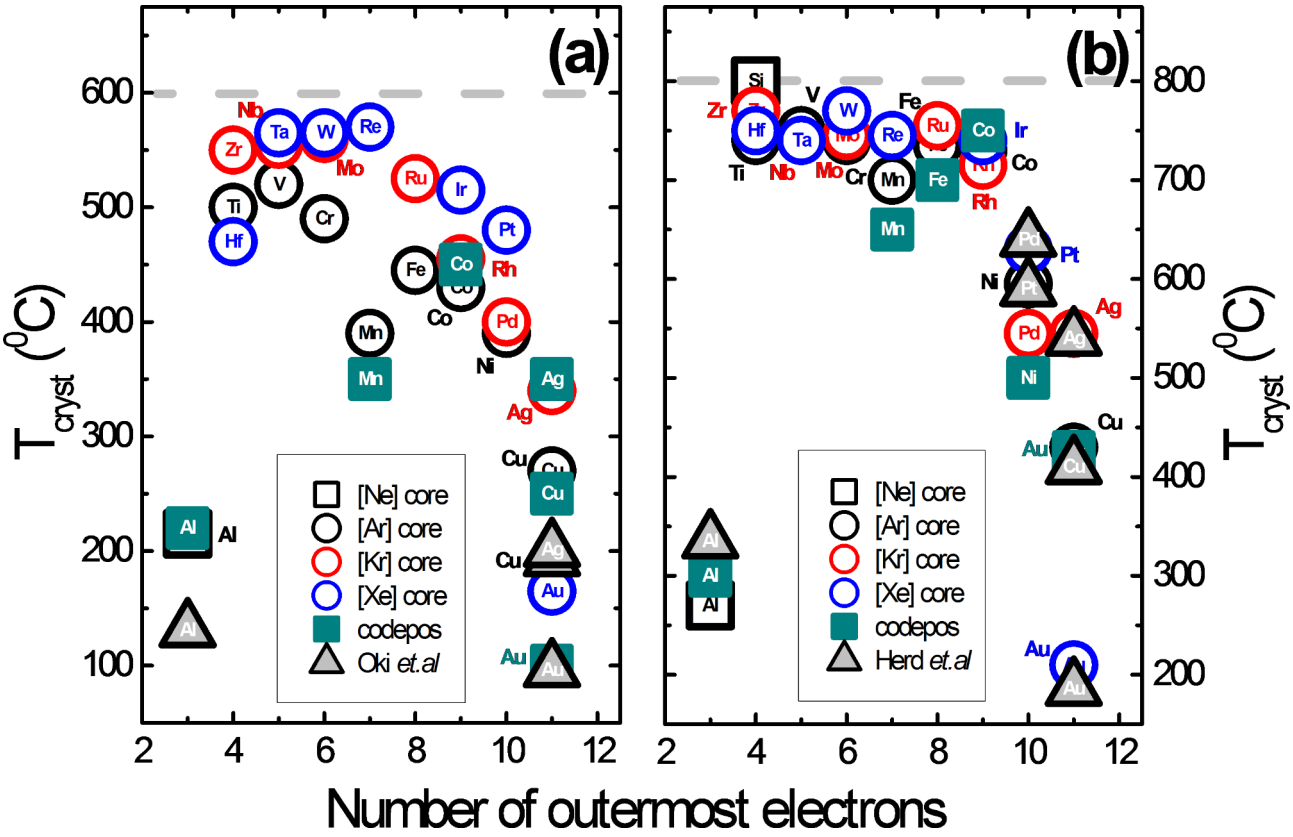

Fig. 3. Crystallization temperature T_{cryst} *versus* the number of outermost electrons (or number of electrons beyond the noble gas core or configuration), as observed in the MIC of amorphous Ge (a) and Si (b) films. The dashed horizontal gray lines indicate the typical T_{cryst} of metal-free Ge (~ 600 °C) and Si (~ 800 °C) films[29,30]. The figures show the results from metal−semiconductor bi-layered samples[29,30] (separated according to the rows the metals occupy in the Periodic Table of Elements), along with the data from codeposited films (codepos− this work, Oki et al.[4] in (a), and Herd et al.[6] in (b)).

One additional version of Fig. 3 that includes the data of Ge films codeposited with Zn and Cd ($n_{out} = 12$), Sn and Pb ($n_{out} = 14$), and Sb and Bi ($n_{out} = 15$) is presented in SuppInfo_Part3. Once again, the figure displays some data scatter (mainly because of variations in the metal concentration of the films), but the T_{cryst} *versus* n_{out} behavior remains exactly the same. Unfortunately, no equivalent data (regarding higher n_{out} values) were found for the Si films.

The discussion of Fig. 3 will be made by initially considering some specific features of the results and, then, by proposing a phenomenological model that explains the overall T_{cryst}−n_{out} behavior.

With the exception of the Al- and Mn-related data, and by adopting an arbitrary decrease of more than 10% in the T_{cryst} of the metal-free films, there is a clear reduction in the crystallization temperatures of the metal−Ge samples presenting $n_{out} \geq 8$ and of the metal−Si samples with $n_{out} \geq 10$. The effect seems to be less abrupt in the metal−Ge samples (Fig. 3a) and, within the $T_{cryst} \pm 50$–100 °C range, no significant differences can be noticed in the metals belonging to the **[Ar]**, **[Kr]**, and **[Xe] core** groups (Fig. 3a, b). Obviously, these aspects must be related to the electronic structure of the elements. In the case of the semiconductors: Ge has the [Ar] $3d^{10}$ $4s^2$ $4p^2$ electron configuration and Si ≡ [Ne] $3s^2$ $3p^2$. Concerning the transition metals (or *d*-block elements): they present *d* shells (3*d*, or 4*d*, or 5*d* successively filled with up to 10 electrons), that are known to project well out to the periphery of the atoms (or ions)[45]. As a consequence, the electrons occupying the *d* orbitals are strongly influenced by the surroundings (and vice-versa), and many of the properties of a transition metal atom (or ion), with a partially filled *d* shell, are quite sensitive to the number and arrangement of the *d* electrons present[42,45]. Within this context, the resemblance of Ge (that belongs to the **[Ar] core** group) with the *d*-block elements may be associated with the observed smooth T_{cryst}−n_{out} behavior (Fig. 3a), at the same time that the half-filled 3*d* orbital of Mn may explain the incongruous T_{cryst} of the Mn−Ge sample. Actually, the distinctive $3d^5$ orbital of Mn may also be the reason for the comparatively lower T_{cryst} of the Mn−Si sample (Fig. 3b) that, in contrast to the other d^5 metals, some of them: were not investigated (Tc ≡ [Kr] $4d^5$ $5s^2$), or either exhibit a half-filled most external *s* orbital (Cr ≡ [Ar] $3d^5$ $4s^1$ and Mo ≡ [Kr] $4d^5$ $5s^1$) or present filled f^{14} and s^2 orbitals (Re ≡ [Xe] $4f^{14}$ $4d^5$ $5s^2$). Moreover, manganese exhibits a rather low cohesive energy, and one of its most common stereochemistries is the Mn II, in which Mn^{2+} ions are able to occupy interstitial spaces in amorphous networks[45]. With respect to Al, it is within the best metals in decreasing the T_{cryst} of the Ge and Si films and, different from all the other metals considered in the study of MIC (Fig. 3a, b), Al (≡ [Ne] $3s^2$ $3p^1$) is the only one that presents the outermost

p orbital. More specifically, while some metals were not considered (Ga ≡ [Ar] $3d^{10}\,4s^2\,4p^1$, In ≡ [Kr] $4d^{10}\,5s^2\,5p^1$, and Tl ≡ [Ar] $4f^{14}\,5d^{10}\,6s^2\,6p^1$) in the study (Fig. 3a, b), others were probed only in the Ge films (SuppInfo_Part3) presenting *p* orbitals with: either 2 (Sn ≡ [Kr] $4d^{10}\,5s^2\,5p^2$ and Pb ≡ [Xe] $4f^{14}\,5d^{10}\,6s^2\,6p^2$) or 3 electrons (Sb ≡ [Kr] $4d^{10}\,5s^2\,5p^3$ and Bi ≡ [Xe] $4f^{14}\,5d^{10}\,6s^2\,6p^3$). In combination, the Al−Ge and Al−Si results (along with those shown by the Sn−Ge, Pb−Ge, Sb−Ge, and Bi−Ge samples) suggest the influence of the *p* orbitals (in terms of their typical shape and extent) in the MIC phenomenon. Provided that the experimental data of Fig. 3 are accurate enough to describe the crystallization features of the Ge and Si films, the above discussion highlights the importance of the electron configuration of the metal−semiconductor atoms in the MIC mechanisms.

The concept of electron orbitals relating the bonding of atoms (as originated from the solution of the Schroedinger equation for the hydrogen atom) is very effective when studying molecules and solids[46]. The proper management of the concept can provide a detailed description of the main properties of molecules and solids and, in certain cases, anticipate new−unusual materials characteristics. This is no different when studying the MIC phenomenon in which the idea of electron configuration and atom bonding is perfectly compatible with both the short- and long-range order present, respectively, in the amorphous (as-prepared) and crystalline (after MIC) Ge and Si films. Independently, metals and semiconductors behave in their own way because of the interaction between their atoms—as imposed by their electron configuration and orbitals details. In the former case, the consecutive electron filling of the *d* orbitals makes the transition metals very unique presenting a high optical reflectivity and superior electrical conductivity, for example. There is no ionic contribution in their atom bonding and, since there are neither sufficient electrons nor sufficient orbitals, it is impossible to have two-electron covalent bonds between all adjacent pairs of atoms[46]. Put in other words, metal atoms are united by metallic (delocalized) bondings, whose main characteristics are the sharing of electrons between many atoms and no distinction between occupied (bonding) and unoccupied (anti-bonding) orbitals. The semiconductors Ge and Si, on the contrary, are the consequence of the interaction between their outermost s^2p^2 orbitals (more properly, hybrid sp^3 orbitals), rendering a covalent-type (localized) bonding between the Ge or Si atoms. They are non-metallic materials (whose electrons can occupy either the bonding or anti-bonding orbitals) that present a modest optical reflectivity (and well-defined optical properties[47]), and that are able to conduct electricity by virtue of thermal excitation of electrons across the energy gap between occupied and non-occupied states[46,48]. Most of all, the interaction between (metal and/or semiconductor) atoms will be mutually influenced by the overlapping of their (outermost) electron orbitals as well as by their individual nature.

Applied to the MIC phenomenon, regardless of the samples characteristics (codeposited or layered), the physical proximity of the metal and semiconductor atoms (chemically bonded, or not) will provoke their interaction that, ultimately, will give rise to the amorphous-to-crystalline transformation of the Ge and Si films. Accordingly, the number of available metal species (or metal concentration) should be as much as necessary to modify the atom environment of the amorphous films. Initially, in the absence of any external energy supply the presence of metal atoms augments the structural disorder of the films. It happens because of defects (originated in order to adjust the metal−semiconductor interface or to accommodate interstitial foreign species) or simply because of unintentional metal−semiconductor bonds[49]. As energy is supplied (by thermal annealing, for instance) the inherent structural disorder of the films partially recovers and the MIC phenomenon takes place. Even though amorphous Ge and Si present practically the same short-range order (comprised by local tetrahedral bonding units) of their crystalline counterparts, this local order is randomly connected and the Ge−Ge and Si−Si bonds are metastable (or under non-equilibrium conditions)[50,51]. The arrangement of these Ge−Ge or Si−Si (or even metal−semiconductor) bonds facilitates the atom reordering required to attain crystallization. In fact, this amorphous-to-crystalline transformation can be accomplished by simple thermal annealing [(as in Fig. 1c, g), but the process is much more effective if assisted by the presence of metal species (Fig. 1a, e). In this case, the metal−semiconductor interaction acts by rearranging the Ge−Ge or Si−Si bonds until they reach the most stable (crystalline) condition. This interaction seems to be more effective when the number of outermost electrons $n_{out} \geq 8$—corresponding to metals presenting at least 6 electrons in the *d* orbitals—in the Ge films (Fig. 3a), and when $n_{out} \geq 10$—denoting metals with the *d* orbitals complete (Pd ≡ [Kr] $4d^{10}$) or partially complete (Ni ≡ [Ar] $3d^8\,4s^2$ or [Ar] $3d^9\,4s^1$, and Pt ≡ [Xe] $4f^{14}\,5d^9\,6s^1$)—in the Si films (Fig. 3b). Apparently, owing to their metallic-bond character the "extra" electrons occupying the more than half-filled *d* orbitals (i.e., $d^{\geq 6}$), together with those in the *s* orbitals, are "free" to move around[45,52] promoting the atom-bonding rearrangement necessary to crystallize the Ge and Si films. These "extra−free" electrons promote some shield in the electrostatic interaction responsible for the Ge−Ge or Si−Si bonds that become unstable and, therefore, facilitate the atom-bonding process. Since these electrons determine the atoms main characteristics and present a very limited range of spatial influence, rigorously, they are not extra not even free, but the "extra−free" designation is adequate to conceive their role in the MIC mechanism. This partial shielding effect, also known as Coulomb screening[53], was originally proposed as a bond-breaking model to describe the development of silicides as induced by near-noble metals in crystalline Si[54,55] and, since then, it has been considered to explain the crystallization of Au−Ge films[56] and many other metal−semiconductor systems[57]. In contrast to the present work, however, none of these previous studies considered the specifics of the atoms involved nor the MIC of codeposited and layered samples as obtained from various different metal species. Besides, considering the intrinsic (crystal-like) short-range order of the amorphous Ge and Si films and the comparatively higher energy required to break a chemical bond it seems unlikely that a crystallization mechanism entirely based on a bond-breaking model applies. Occasionally, the break of Ge−Ge or Si−Si (or even metal−Ge or metal−Si) bonds can occur during the amorphous-to-crystalline transformation but, definitively, it should not represent the (sole) main process.

Still related to this atom-bonding rearrangement mechanism, as promoted by the "extra−free" electrons present in the metal atoms, it is not clear if the metal species need to be bonded to the Ge or Si atoms or simply be nearby (occupying an interstitial site, for example[56]). Obviously, the metal−semiconductor interaction

will be different if the metal atoms are bonded or not but, provided that the metal "extra–free" electrons alter the originally disordered Ge−Ge or Si−Si bonds, this will suffice to advance the amorphous-to-crystalline transformation. In this case, the atom-bonding rearrangement mechanism will take place in the regions influenced by the wavefunctions of the metal "extra−free" electrons. Furthermore, the MIC mechanism will be determined by n_{out} as well as by the specifics of each atomic orbital involved[45,52]—such as those involving the *p* orbitals (i.e.: Al, Sn, Pb, Sb, and Bi, for example—SuppInfo_Part3). Insofar as the local bondings are rearranged and the Ge or Si crystallites develop, the crystallization process advances by squeezing out the metal species because of their low solubility in crystalline Ge and Si hosts, and the MIC mechanism continues. This is in accord with the metal diffusion usually verified in the metal−semiconductor layered samples[7,57], and suggests that the MIC mechanism pave the way to the mass transport phenomena (and not the contrary).

Another way to conceive the MIC of the Ge and Si films involves the energy aspects of their amorphous-to-crystalline transformation as depicted in Fig. 4. The figure displays the traditional ball-and-stick models relating the atomic structure of the tetrahedrally bonded Ge or Si atoms in the amorphous state (Fig. 4 (1) and (2)) and after crystallization (Fig. 4 (3)). An energy *versus* reaction coordinate diagram is also shown, clearly denoting the main steps of the amorphous-to-crystalline transformation of the Ge or Si films (with and without metal species).

From the thermodynamic point of view, the amorphous-to-crystalline transformation of the Ge and Si films involves the minimization of their total energy by overcoming an energy barrier that is usually associated with the intrinsic structural disorder and/or due to the presence of defects[50,51,58]. Since the process is thermally activated, the magnitude of this energy barrier—separating the amorphous (metastable) from the crystalline (most stable) states—is described by an activation energy E_A. Applied to the MIC phenomenon, this is shown in Fig. 4 by clearly indicating the activation energies corresponding to the metal-free ($E_A^{(1)}$) and metal-containing ($E_A^{(2)}$) cases. The contrasting $E_A^{(1)} > E_A^{(2)}$ representation is not fortuitous and it arises from the comparatively lower temperatures required to induce the crystallization of the metal-containing Ge or Si films (Figs. 1a and e and 2, and Fig. 3) and, particularly, from the activation energy values determined experimentally[29–32]. In fact, whereas the E_A's of the metal-free Ge and Si films stay in the 3−4 eV range, they can be systematically reduced down to ~ 1.5 eV in the metal−semiconductor samples (see SuppInfo_Part4). Such a decrease is consistent with the atom-bonding rearrangement mechanism, according to which the energy constrains (or energy barrier heights) are expected to be comparatively lower. This amorphous-to-crystalline transformation picture is strictly related to the crystallization temperature T_{cryst} and, hence, it can be associated with the variations observed in the T_{cryst} of either the metal-free or metal-containing Ge or Si samples. In order to do that, it is important to define a (very speculative) ideal sample condition denoting the least activation energy (and therefore the lowest T_{cryst} value), as obtained from various authors and experimental conditions. Accordingly, any data dispersion beyond the $T_{cryst} \pm 50$–100 °C range (comprising some data dispersion, the experimental error, and small variations in defining T_{cryst}) might be related with: (a) in the metal-free samples − the intrinsic structural disorder of the Ge or Si films due to the sample production and processing details (as in Fig. 1c and g, for example); (b) in the metal-deficient samples—a mixed metal-free−metal-containing atomic environment, in which there are not enough metal "extra−free" electrons, such that the energy barrier is expected to stay between the $E_A^{(1)}$ and $E_A^{(2)}$ values as suggested by the T_{cryst} of the Ge film containing only 0.8 at% of Pb (Fig. 1a and SuppInfo_Part3), and by the still decreasing T_{cryst} presented by the codeposited SiAu film, for example (Figs. 1f and 3b); and (c) in the metal-rich samples—again, an energy barrier height between $E_A^{(1)}$ and $E_A^{(2)}$ that is necessary to equalize the increased structural disorder caused by the excess of metal species or, alternatively, to compensate for the energy spent during the development of unwanted (germanide/silicide?) phases—see the T_{cryst} of the Si films with Ni and Pd in Fig. 3b, for example, in which the higher T_{cryst}'s may suggest an increased amount of metal.

In combination with the concept of the outermost ("extra−free") electrons and the atom-bonding rearrangement mechanism, the above discussion provides a comprehensive description of the metal-induced crystallization of Ge and Si amorphous films. In its present form, this phenomenological model is simple (based on standard chemical concepts), inclusive (comprising the results of both codeposited and bi-layered samples), and very consistent (with the available literature and experimental data uncertainty). In view of that, we expect it can be useful in advancing the research efforts regarding the production of (poly-)crystalline Ge or Si films by means of reduced thermal budgets, by proposing new metal−semiconductor combinations and/or sample processing practices. To the extent that these goals are met, and depending on the desired technological application, new challenges will comprise the development of mono-crystalline films as well as the removal of any (inadvertent) metal excess.

Conclusions

Since its first observation, the metal-induced crystallization (or simply MIC) of amorphous Ge and Si films represents a scientific challenge that, eventually, can have a great technological impact in the microelectronics and photovoltaics industries, for example. Roughly, the MIC phenomenon relies on a metal−Ge or metal−Si combination that, assisted by an external energy input (usually, thermally-based) can, in the best scenario, decrease the crystallization temperature T_{cryst} of the amorphous Ge or Si films from ~ 600–800 °C down to ~ 200 °C. As a result, the MIC phenomenon has been the subject of many research efforts that provided lots of information without, however, reaching to a simple−unified explanation. Driven by these aspects, this work considered the MIC results of several codeposited and bi-layered metal−Ge and metal−Si samples that were presented and discussed in detail (i.e., in terms of the metal nature and amount, the temperature−time processing details, and regarding the crystallization criteria).

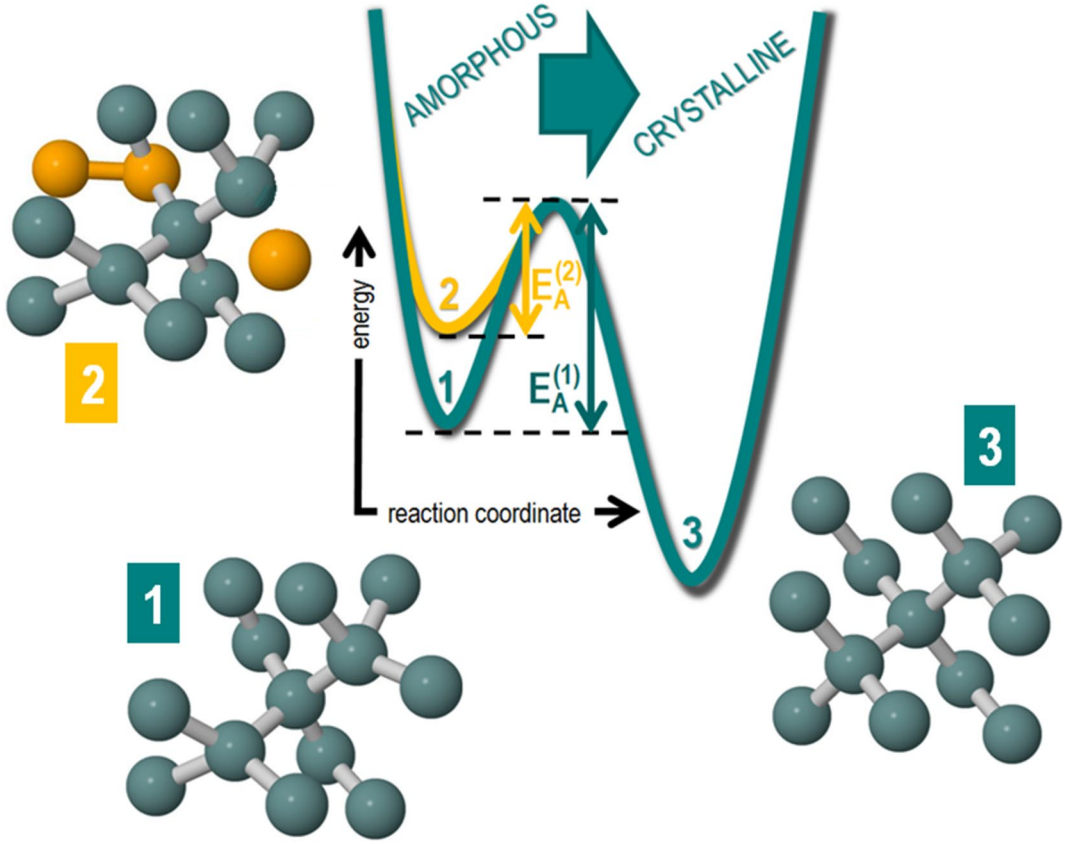

Fig. 4. Artistic view of the amorphous-to-crystalline transformation taking place in Ge or Si films. The picture illustrates the typical ball-and-stick model of tetrahedrally bonded Ge or Si atoms (dark spheres): (1) in the amorphous (metastable) state, (2) the same as before, but in combination with metal atoms (light spheres) either bonded or occupying an interstitial space, and (3) in the crystalline (most stable) state. The corresponding (amorphous-to-crystalline) energy diagram shows the activation energies i.e., the minimum energy required to transform the amorphous metal-free ($E_A^{(1)}$) and metal-containing ($E_A^{(2)}$) films into crystalline Ge or Si films.

In view of this comprehensive data analysis and discussion, it was possible to propose a simple phenomenological model to account for the MIC phenomenon. The model is based on the electron distribution, the electron orbitals main features, and the bonding character of the metal, Ge, and Si atoms to describe the metal–semiconductor interaction. The local order of the amorphous Ge and Si lattices, as influenced by this metal–semiconductor interaction, has also been taken into consideration (by means of their chemical and thermodynamic aspects) in order to explain the amorphous-to-crystalline transformation of the Ge and Si films. According to the model, the metal species presenting "extra–free" electrons into their outermost orbitals—as defined by the n_{out} quantity—are the most effective in promoting an atom-bonding rearrangement mechanism and, therefore, in reducing the T_{cryst} of the amorphous films. The model clearly indicates the main chemical–thermodynamic–structural aspects behind the MIC phenomenon and, most of all, it is consistent with a substantial ensemble of experimental results. Finally, we hope the ideas presented in this phenomenological model can contribute to advance–improve the production of (poly-)crystalline Ge or Si films via reduced thermal budgets.

Materials and methods

Metal–semiconductor codeposited films

Films based on the Ge and Si semiconductors were prepared in a high vacuum chamber (base pressure ~ 2×10^{-6} Torr) by radio frequency sputtering polycrystalline Ge or Si targets in an atmosphere of pure argon (working pressure ~ 1.5×10^{-3} Torr). Typically, the deposition runs were 1–2 h long rendering ~ 500 nm thick amorphous films (as indicated by Raman spectroscopy – see below), that were deposited onto fused silica substrates (kept at 100 ± 10 °C). The insertion of metallic species into the amorphous films was achieved by partially covering the Ge or Si targets with small pieces of the desired metal, such that the metal concentration was adjusted by simply varying the relative metal-to-semiconductor target area, in a process known as cosputtering[59]. Even though the reliability of the procedure, the exact metal content in the amorphous Ge and Si films was confirmed by energy dispersive x-ray EDX analysis (see SuppInfo_Part5 for further details). In all deposition runs, very high purity precursors were considered: argon gas (99.9995% or 5N5 pure), Ge and Si solid targets (5N), and metallic

species (at least 4N5). After deposition, the films were submitted to cumulative isochronal (15 min each) thermal annealing treatments at increasing temperatures (~150–750 °C range) under a continuous flow of either argon or nitrogen.

Raman scattering spectroscopy represents one of the most convenient techniques to probe variations in the atomic structure of various classes of materials and it has been extensively considered in the characterization of the present films[60,61]. The measurements were carried out at room-conditions, under the backscattering geometry, by exciting the films with 632.8 nm laser radiation. Given the high sensitivity of the amorphous films to laser radiation, and in order to avoid unintentional crystallization[62], a laser power density of 200 μW/μm^2 was adopted in all measurements. The experimental work included the acquisition of various spectra and the measurement of different regions of the very same film—in the pure and metal-containing forms, as-deposited and after each annealing step. The proper analysis of the so obtained Raman spectra can be used to identify the relative composition as well as details relating the atomic structure of the films[63]. Roughly, this is accomplished by fitting the Raman spectra with either Lorentz or Gaussian functions (or a combination of them), each one associated with contributions that can be due to amorphous or crystalline nature[64]. In the case of the Ge-based films these contributions take place at[65]: ~ 270 ± 5 cm^{-1} (amorphous), in the ~275–295 cm^{-1} range (crystallites with different sizes and/or interface modes), and at ~300 ± 3 cm^{-1} (crystalline). For the Si-based films[65]: at ~470 ± 10 cm^{-1} (amorphous), in the ~480–515 cm^{-1} range (crystallites with different sizes and/or interface modes), and at ~520 ± 5 cm^{-1} (crystalline). The relative amount of these contributions gives a good estimate of the fraction of crystalline structures ($X_{fraction}$) present in the films according to:

$$X_{fraction} = \frac{A_{Xtal}}{A_{Xtal} + 0.8 \cdot A_{amorp}}, \quad (1)$$

where A_{Xtal} and A_{amorp} stand, respectively, for the integrated areas of the crystalline and amorphous phases, and the correction factor 0.8 compensates for differences owing to the light scattering cross-sections of the amorphous and crystalline contributions[66,67]. Following this approach, for the present purposes, the crystallization temperature T_{cryst} of each Ge- and Si-based film was associated to the middle temperature between $X_{fraction} = 0$ and $X_{fraction} \neq 0$ by considering a ±50 °C uncertainty. Additional information regarding the preparation, thermal annealing, and detailed Raman scattering analyses can be found elsewhere: Ge–Al films[25,49,68], Ge–Mn [49,69,70], Ge–Co[49,71], Ge–Sn[28], Si–Al films[27], Si–Mn[49,72], Si–Fe[49,73], Si–Co[49,71], and Si–Ni[26,49,74,75].

Metal–semiconductor bi-layer samples[29,30]

These samples correspond to 30 nm thick metal films (Al, Ti, V, Cr, Mn, Fe, Co, Ni, Cu, Zr, Nb, Mo, Ru, Rh, Pd, Ag, Hf, Ta, W, Re, Ir, Pt or Au) on top of 200 nm thick amorphous Ge or Si films. All films were deposited by sputtering the metal, Ge or Si solid targets (in a pure argon plasma) onto crystalline Si(100) substrates previously covered with a thermally-grown SiO_2 cap (100 nm thick).

The atomic structure of the samples was studied by in-situ x-ray diffraction measurements in a 14° 2θ range centered around 32° (for the metal–Ge samples, corresponding to Ge(220)) or 55° (metal–Si, Si(111)). The experiments were performed at the Brookhaven National Laboratory (X20C beam line) by means of 6.9 keV x-ray monochromatic radiation and 1.5% energy resolution.

The amorphous-to-crystalline transformation was studied by annealing the samples from 100 to 900 °C (fixed rate of 3 °C/s) in a purified He atmosphere. The crystallization temperatures, as presented by Knaepen et al., correspond to those at which the rate of increase of either the Ge(220) or Si(111) diffraction peak intensity was maximum. The crystallization kinetics of a few selected samples was investigated by additional ramp rates of 1, 5, 9, and 27 °C/s. Further information relating the preparation and characterization of the metal–semiconductor bi-layer samples can be found elsewhere[29,30].

Data availability

All data generated or analysed during this study are included in this published article [and its supplementary information files].

Received: 30 August 2024; Accepted: 2 December 2024
Published online: 28 December 2024

References

1. Gilles, J. & van Cakenberghe, J. Photoconductivity and crystal size in evaporated layers of cadmium sulphide. *Nature* **182**, 862–863. https://doi.org/10.1038/182862b0 (1958).
2. Vecht, A. & Apling, A. A new method of recrystallizing CdS thin films. *phys. stat. sol.* **3**, 1238–1246. https://doi.org/10.1002/pssb.19630030706 (1963).
3. Vecht, A. Methods of activating and recrystallizing thin films of II-VI compounds. In *Physics of Thin Films, Vol 3* (eds. Hass, G. & Thun, R. E.) (Academic Press, 1966). Library of Congress Catalog Card Number 63-16561 .
4. Oki, F., Ogawa, Y. & Fujiki, Y. Effect of deposited metals on the crystallization temperature of amorphous germanium film. *Jpn. J. Appl. Phys.* **8**, 1056. https://doi.org/10.1143/JJAP.8.1056 (1969).
5. Bosnell, J. R. & Voisey, U. C. The influence of contact materials on the conduction crystallization temperature and electrical properties of amorphous germanium, silicon and boron films. *Thin Solid Films* **6**, 161–166. https://doi.org/10.1016/0040-6090(70)90036-2 (1970).
6. Herd, S. R., Chaudhari, P. & Brodsky, M. H. Metal contact induced crystallization in films of amorphous silicon and germanium. *J. Non-Cryst. Sol.* **7**, 309–327. https://doi.org/10.1016/0022-3093(72)90267-0 (1972).
7. Wang, Z., Jeurgens, L. P. H. & Mittemeijer, E. J. Introduction to metal-induced crystallization (Chap 1). In *Metal-induced Crystallization: Fundamentals and Applications* (eds. Wang, Z. et al.) (Pan Stanford Pub., 2015).

8. Jang, J. et al. Electric-field-enhanced crystallization of amorphous silicon. *Nature* **395**, 481–483. https://doi.org/10.1038/26711 (1998).
9. Murley, D., Young, N., Trainor, M. & McCulloch, D. An investigation of laser annealed and metal-induced crystallized polycrystalline silicon thin-film transistors. *IEEE Trans. Elect. Dev.* **48**, 1145–1151. https://doi.org/10.1109/16.925240 (2001).
10. Ahn, J. H., Lee, J. N., Kim, Y. C. & Ahn, B. T. Microwave-induced low-temperature crystallization of amorphous Si thin films. *Curr. Appl. Phys.* **2**, 135–139. https://doi.org/10.1016/S1567-1739(01)00085-2 (2002).
11. Meng, Z., Wang, M. & Wong, M. High performance low temperature metal-induced unilaterally crystallized polycrystalline silicon thin film transistors for system-on-panel applications. *IEEE Trans. Elect. Dev.* **47**, 404–409. https://doi.org/10.1109/16.822287 (2000).
12. Wong, M. et al. Applications of metal-induced crystallization polycrystalline silicon for advanced flat-panel displays (Chap 6). In *Metal-induced Crystallization: Fundamentals and Applications* (eds. Wang, Z. et al.) (Pan Stanford Pub., 2015).
13. Her, Y. C., Jean, S. T. & Wu, J. L. Crystallization kinetics and recording mechanism of a-Si/Ni bilayer for write-once blue-ray recording. *J. Appl. Phys.* **102**, 093503–093507. https://doi.org/10.1063/1.2802992 (2007).
14. Her, Y. C., Chen, J. H., Tsai, M. H. & Tu, W. T. Nickel-induced crystallization of amorphous Ge film for blue-ray recording under thermal annealing and pulsed laser irradiation. *J. Appl. Phys.* **106**, 023530–023535. https://doi.org/10.1063/1.3183956 (2009).
15. Tsaur, B. Y., Turner, G. W. & Fan, J. C. C. Efficient Si solar cells by low-temperature solid-phase epitaxy. *Appl. Phys. Lett.* **39**, 749–751. https://doi.org/10.1063/1.92878 (1981).
16. Gordon, I., Carnel, L., van Gestel, D., Beaucarne, G. & Poortmans, J. Fabrication and characterization of highly efficient thin-film polycrystalline-silicon solar cells based on aluminium-induced crystallization. *Thin Solid Films*. **516**, 6984–6988. https://doi.org/10.1016/j.tsf.2007.12.114 (2008).
17. Konno, T. & Sinclair, R. Crystallization of silicon in aluminium/amorphous-silicon multilayers. *Philos. Mag. B*. **66**, 749–765. https://doi.org/10.1080/13642819208220126 (1992).
18. Nast, O., Puzzer, T., Koschier, L. M., Sproul, A. B. & Wenham, S. R. Aluminum-induced crystallization of amorphous silicon on glass substrates above and below the eutectic temperature. *Appl. Phys. Lett.* **73**, 3214–3216. https://doi.org/10.1063/1.122722 (1998).
19. Wang, J. Y., Wang, Z., Jeurgens, L. P. H. & Mittemeijer, E. J. Diffusion, crystallization, and layer exchange upon low-temperature annealing of amorphous Si/polycrystalline Al layered structures (Chap 3). In *Metal-induced Crystallization: Fundamentals and Applications* (eds. Wang, Z. et al.) (Pan Stanford Pub., 2015).
20. Zharkov, S. M. et al. Thermokinetic study of aluminum-induced crystallization of a-Si: the effect of Al layer thickness. *Nanomaterials* **13**, 2925–2924. https://doi.org/10.3390/nano13222925 (2023).
21. Jin, Z., Bhat, G. A., Yeung, M., Kwok, H. S. & Wong, M. Nickel induced crystallization of amorphous silicon thin films. *J. Appl. Phys.* **84**, 194–200. https://doi.org/10.1063/1.368016 (1998).
22. Miyasaka, M., Makihira, K., Asano, T., Polychroniadis, E. & Stoemenos, J. In-situ observation of nickel metal-induced lateral crystallization of amorphous silicon thin films. *Appl. Phys. Lett.* **80**, 944–946. https://doi.org/10.1063/1.1447014 (2002).
23. Miyasaka, M. et al. Structural properties of nickel metal-induced laterally crystallized silicon films and their improvement using excimer laser annealing. *Jpn J. Appl. Phys.* **42**, 2592–2599. https://doi.org/10.1143/JJAP.42.2592 (2003).
24. Vouroutzis, N. et al. Structural characterization of poly-Si films crystallized by Ni metal induced lateral crystallization. *Sci. Rep.* **9**, 2844-8. https://doi.org/10.1038/s41598-019-39503-9 (2019).
25. Zanatta, A. R. & Chambouleyron, I. Low-temperature Al-induced crystallization of amorphous Ge. *J. Appl. Phys.* **97**, 094914-11. https://doi.org/10.1063/1.1889227 (2005).
26. Ferri, F. A., Zanatta, A. R. & Chambouleyron, I. Metal-induced nanocrystalline structures in Ni-containing amorphous silicon thin films. *J. Appl. Phys.* **100**, 094311–094317. https://doi.org/10.1063/1.2362877 (2006).
27. Zanatta, A. R. & Kordesch, M. E. On the structural-optical properties of Al-containing amorphous Si thin films and the metal-induced crystallization phenomenon. *J. Appl. Phys.* **116**, 073511–073517. https://doi.org/10.1063/1.4893654 (2014).
28. Zanatta, A. R. The role of tin atoms on the crystallization of amorphous germanium films. *Mater. Chem. Phys.* **306**, 128045–128047. https://doi.org/10.1016/j.matchemphys.2023.128045 (2023).
29. Knaepen, W., Detavernier, C., van Meirhaeghe, R. L., Sweet, J. J. & Lavoie, C. In-situ x-ray diffraction study of metal-induced crystallization of amorphous silicon. *Thin Solid Films*. **516**, 4946–4952. https://doi.org/10.1016/j.tsf.2007.09.037 (2008).
30. Knaepen, W. et al. In situ x-ray diffraction study of metal-induced crystallization of amorphous germanium. *J. Appl. Phys.* **105**, 083532–083537. https://doi.org/10.1063/1.3110722 (2009).
31. Blum, N. A. & Feldman, C. The crystallization of amorphous silicon films. *J. Non-Cryst. Sol.* **11**, 242–246. https://doi.org/10.1016/0022-3093(72)90006-3 (1972).
32. Blum, N. A. & Feldman, C. The crystallization of amorphous germanium films. *J. Non-Cryst. Sol.* **22**, 29–35. https://doi.org/10.1016/0022-3093(76)90004-1 (1976).
33. Toko, K., Oya, N., Saitoh, N., Yoshizawa, N. & Suemasu, T. 70 °C synthesis of high-Sn content (25%) GeSn on insulator by Sn-induced crystallization of amorphous Ge. *Appl. Phys. Lett.* **106**, 082109–082104. https://doi.org/10.1063/1.4913744 (2015).
34. Toko, K. & Suemasu, T. Metal-induced layer exchange of group IV materials. *J. Phys. D: Appl. Phys.* **53**, 373002–373017. https://doi.org/10.1088/1361-6463/ab91ec (2020).
35. Ishiyama, T., Igura, K., Suemasu, T. & Toko, K. Metal-induced lateral crystallization of germanium thin films. *Mater. Design*. **232**, 112116–112117. https://doi.org/10.1016/j.matdes.2023.112116 (2023).
36. Lide, D. R. *CRC Handbook of Chemistry & Physics* (Taylor&Francis Group, 2007).
37. Various authors. *Bulletin of Alloy Phase Diagrams* (ASM International, 1980–1989).
38. Gaudet, S., Detavernier, C., Kellock, A. J., Desjardins, P. & Lavoie, C. Thin film reaction of transition metals with germanium. *J. Vac. Sci. Technol. A* **24**, 474–485. https://doi.org/10.1116/1.2191861 (2006).
39. Ottaviani, G. Review of binary alloy formation by thin film interactions. *J. Vac. Sci. Technol.* **16**, 1112–1119. https://doi.org/10.1116/1.570170 (1979).
40. Various INSPEC, the Institution of Electrical Engineers, UK. In *Properties of Metal Silicides* (eds. Maex, K. & van Rossum, M.) (Wiley, 1995).
41. Most of the data concerning the T_{Debye} were achieved from https://www.knowledgedoor.com/ and from the citations presented there (Ho, C. Y., Powell, R. W. & Liley, P. E. Thermal conductivity of the elements: A comprehensive review. J. Phys. & Chem. Ref. Data 3-Supp1 1-796. ISBN 13 978 0883182161) (1974).
42. Atkins, P. W. *Physical Chemistry* (Oxford Univ Press, 1994).
43. Brodsky, M. H. & Turnbull, D. Low temperature eutectic induced crystallization of amorphous materials. Bull Amer Phys Soc 16 304. No doi (not even any digital-electronic media) available. The phrase between the quotation marks is usually associated with this reference. However, it corresponds to the abstract (100-words) of a paper presented in the *American Physical Society* meeting, with absolute no discussion. Apparently, the study was revisited in Ref [6] but, again, the *formation of a low-temperature eutectic melt* statement has never been shown (1971).
44. Blakemore, J. S. *Lattice dynamics (Chap 2), in Solid State Physics* (Cambridge Univ Press, 1985).
45. Cotton, F. A., Wilkinson, G. & Gaus, P. L. *Basic Inorganic Chemistry* (Wiley, 1995).
46. Cox, P. A. *The Electronic Structure and Chemistry of Solids* (Oxford Univ Press, 1987).
47. Zanatta, A. R. Revisiting the optical bandgap of semiconductors and the proposal of a unified methodology to its determination. *Sci. Rep.* **9**, 11225. https://doi.org/10.1038/s41598-019-47670-y (2019).

48. Kittel, C. Semiconductor crystals (Chap 8).In *Introduction to Solid State Physics* (Willey, 1976).
49. Zanatta, A. R. & Ferri, F. A. Metal-induced crystallization by homogeneous insertion of metallic species in amorphous semiconductors (Chap 4). In *Metal-induced Crystallization: Fundamentals and Applications* (eds. Wang, Z. et al.) (Pan Stanford Pub., 2015).
50. Mott, N. F. & Davis, E. A. *Electronic Processes in Non-crystalline Materials* (Clarendon Press, 1979).
51. Street, R. A. *Hydrogenated Amorphous Silicon* (Cambridge Univ Press, 1991).
52. Harrison, W. A. *Electronic Structure and the Properties of Solids—The Physics of the Chemical Bond* (Freeman, W. H. & Comp, 1980).
53. Hiraki, A. Low temperature reactions at Si/metal interfaces: what is going on at the interfaces? *Surf. Sci. Rep.* **3**, 357–412. https://doi.org/10.1016/0167-5729(84)90003-7 (1984).
54. Tu, K. N. Selective growth of metal-rich silicide of near-noble metals. *Appl. Phys. Lett.* **27**, 221–224. https://doi.org/10.1063/1.88436 (1975).
55. Hiraki, A. A model on the mechanism of room temperature interfacial intermixing reaction in various metal-semiconductor couples: what triggers the reaction? *J. Electrochem. Soc.* **127**, 2662–2665. https://doi.org/10.1149/1.2129568 (1980).
56. Tan, Z., Heald, S. M., Rapposch, M., Bouldin, C. E. & Woicik, J. C. Gold-induced germanium crystallization. *Phys. Rev. B.* **46**, 9505–9510. https://doi.org/10.1103/PhysRevB.46.9505 (1992).
57. Wang, Z., Jeurgens, L. P. H. & Mittemeijer, E. J. Thermodynamics and atomic mechanisms of metal-induced crystallization of amorphous semiconductors at low temperature (Chap 2). In *Metal-induced Crystallization: Fundamentals and Applications* (eds. Wang, Z. et al.) (Pan Stanford Pub., 2015).
58. Tanaka, K., Maruyama, E., Shimada, T. & Okamoto, H. *Amorphous Silicon* (Wiley, 1999).
59. Vossen, J. L. & Cuomo, J. J. Glow discharge sputter deposition (Chapter II-1). In *Thin Film Processes* (eds. Vossen, J. L. & Kern, W.) (Academic Press Inc., 1978).
60. Smith, E. & Dent, G. In *Modern Raman Spectroscopy: A Practical Approach* (John Wiley & Sons, UK). ISBN 0-471-49794-0 (2005).
61. Treado, P. J. & Nelson, M. P. Raman imaging, in *Handbook of Raman Spectroscopy* – Chap 5, Edited by Lewis, I. R. & Edwards H. G. M. (Marcel Dekker Inc., NY). ISBN 0-8247-0557-2 (2001).
62. Zanatta, A. R. & Ribeiro, C. T. M. Laser-induced generation of micrometer-sized luminescent patterns on rare-earth-doped amorphous films. *J. Appl. Phys.* **96**, 5977–5981. https://doi.org/10.1063/1.1794363 (2004).
63. Gouadec, G. & Colomban, P. Raman spectroscopy of nanomaterials: how spectra relate to disorder, particle size and mechanical properties. *Prog Cryst. Growth Charact. Mat.* **53**, 1–56. https://doi.org/10.1016/j.pcrysgrow.2007.01.001 (2007).
64. Smit, C. et al. C. M. determining the material structure of microcrystalline silicon from Raman Spectra. *J. Appl. Phys.* **94**, 3582–3588. https://doi.org/10.1063/1.1596364 (2003).
65. Bermejo, D. & Cardona, M. Raman scattering in pure and hydrogenated amorphous germanium and silicon. *J. Non-Cryst. Sol.* **32**, 405–419. https://doi.org/10.1016/0022-3093(79)90085-1 (1979).
66. Tsu, R., Hernandez, J. G., Chao, S. S., Lee, S. C. & Tanaka, K. Critical volume fraction of crystallinity for conductivity percolation in phosphorus-doped Si:F:H alloys. *Appl. Phys. Lett.* **40**, 534–535. https://doi.org/10.1063/1.93133 (1982).
67. Fujii, M., Hayashi, S. & Yamamoto, K. Growth of Ge microcrystals in SiO_2 thin film matrices: a Raman and electron microscopy study. *Jpn J. Appl. Phys.* **30**, 687–694. https://doi.org/10.1143/JJAP.30.687 (1991).
68. Chambouleyron, I., Fajardo, F. & Zanatta, A. R. Aluminum-induced crystallization of hydrogenated amorphous germanium thin films. *Appl. Phys. Lett.* **79**, 3233–3235. https://doi.org/10.1063/1.1415772 (2001).
69. Ferri, F. A. & Zanatta, A. R. Structural, optical and morphological characterization of amorphous $Ge_{100-x}Mn_x$ films deposited by sputtering. *J. Phys. D: Appl. Phys.* **42**, 035005–035006. https://doi.org/10.1088/0022-3727/42/3/035005 (2009).
70. Ferri, F. A., Pereira-da-Silva, M. A., Zanatta, A. R., Varella, A. L. S. & de Oliveira, A. J. A. Effect of mn concentration and atomic structure on the magnetic properties of Ge thin films. *J. Appl. Phys.* **108**, 113922–113925. https://doi.org/10.1063/1.3520661 (2010).
71. Ferri, F. A. & Pereira-da-Silva, M. A. The composition, structure and optical properties of weakly magnetic Co-containing amorphous Si and Ge films. *Mat. Chem. Phys.* **134**, 153–157. https://doi.org/10.1016/j.matchemphys.2012.02.044 (2012).
72. Ferri, F. A., Pereira-da-Silva, M. A. & Zanatta, A. R. Development of the $MnSi_{1.7}$ phase in Mn-containing Si films. *Mat. Chem. Phys.* **129**, 148–153. https://doi.org/10.1016/j.matchemphys.2011.03.064 (2011).
73. Gallo, I. B. & Zanatta, A. R. Structural-electronic aspects related to the near-infrared light emission of Fe-doped silicon films. *Sol Stat. Commun.* **151**, 587–590. https://doi.org/10.1016/j.ssc.2011.02.012 (2011).
74. Ferri, F. A. & Zanatta, A. R. Influence of film thickness on the crystallization of Ni-doped amorphous silicon samples. *J. Appl. Phys.* **104**, 013534–013535. https://doi.org/10.1063/1.2955457 (2008).
75. Zanatta, A. R., Ingram, D. C. & Kordesch, M. E. Influence of Ni concentration on the crystallization of amorphous Si films and on the development of different Ni-silicide phases. *J. Appl. Phys.* **116**, 123508–123506. https://doi.org/10.1063/1.4896589 (2014).

Acknowledgements

This work was financially supported by the Brazilian agencies CNPq (304569/2021-6) and FAPESP.

Author contributions

A.R.Z. has conceived and conducted the experimental work, and wrote/edited the manuscript.

Competing interests

The authors declare no competing interests.

Additional information

Supplementary Information The online version contains supplementary material available at https://doi.org/10.1038/s41598-024-81981-z.

Correspondence and requests for materials should be addressed to A.R.Z.

Reprints and permissions information is available at www.nature.com/reprints.

Publisher's note Springer Nature remains neutral with regard to jurisdictional claims in published maps and institutional affiliations.